Dendritic attenuation of synaptic potentials and currents: the role of passive membrane properties

Nelson Spruston, David B. Jaffe and Daniel Johnston

The dendritic trees of neurons are structurally and functionally complex integrative units receiving thousands of synaptic inputs that have excitatory and inhibitory, fast and slow, and electrical and biochemical effects. The pattern of activation of these synaptic inputs determines if the neuron will fire an action potential at any given point in time and how it will respond to similar inputs in the future. Two critical factors affect the integrative function of dendrites: the distribution of voltage-gated ion channels in the dendritic tree and the passive electrical properties, or 'electrotonic structure', upon which these active channels are superimposed. The authors review recent data from patch-clamp recordings that provide new estimates of the passive membrane properties of hippocampal neurons, and show, with examples, how these properties affect the shaping and attenuation of synaptic potentials as they propagate in the dendrites, as well as how they affect the measurement of current from synapses located in the dendrites. Voltage-gated channels might influence the measurement of 'passive' membrane properties and, reciprocally, passive membrane properties might affect the activation of voltage-gated channels in dendrites.

Nelson Spruston is at the Abteilung Zellphysiologie, Max-Planck-Institut für Medizinische Forschung, Postfach 103820, D-69028 Heidelberg, Germany, David B. Jaffe is at the Dept of Psychology, Yale University, PO Box 11a-Yale Station, New Haven, CT 06520, USA, and Daniel Johnston is at the Division of Neuroscience, Baylor College of Medicine, 1 Baylor Plaza, Houston, TX 77030, USA.

Early views of the neuron assumed that synaptic inputs in the dendrites propagated passively to the site of initiation of the action potential at the soma or axon hillock. With the demonstration of the presence of voltage-gated ion channels in dendrites, this view is now being questioned. Nevertheless, neurophysiologists continue to benefit from earlier theories for analysing the passive flow of current in cable structures [applied to neurons by Rall in the 1960s and 1970s (Ref. 1)]. These simple models provide the framework for more complex models that take into account the active properties of neuronal dendrites.

In addition to having a theoretical framework, it is also useful to have a means of describing the electrotonic properties measured from a given neuron. The elegance of linear cable theory and the appeal of describing a neuron by the electrotonic length (L) of its equivalent cylinder representation (see Box 1) resulted in the analyses of the electrotonic structure of a number of types of neurons. However, the parameter L is more difficult to determine accurately than was initially believed[2] and applies only to a subset of neurons having restricted branching patterns[1]. Consequently, a number of other methods have been used to describe the electrotonic structure of neurons. These methods are summarized in Box 1. What all of these methods have in common is the need for accurate determination of the passive membrane properties, namely the specific membrane resistivity (R_m) and specific membrane capacitance (C_m).

Perforated patch-clamp estimates of the passive membrane properties of hippocampal neurons

Accurate measurement of R_m is necessary both because of its importance in determining the electrotonic structure of neurons and because of its effects on the timecourse of post-synaptic potentials (PSPs). Membrane resistivity can be determined from the membrane time constant (τ_m) by using the definition of τ_m (Eqn 4, Box 1), since C_m is believed to be a constant, with a value of about 1.0 μF/cm^2 (although recent work suggests slightly lower values[3]). The membrane time constant can be estimated experimentally because it corresponds to the slowest time constant (τ_0) of the passive voltage response to a step current injection (see Eqn 3, Box 1). In addition, the input resistance at the soma (R_N, which is determined by R_m, R_i and the morphology of the neuron) can be measured from the steady-stage voltage response to a step of current.

Early estimates of τ_0 and R_N were made from many types of neurons using conventional microelectrode recordings. Because the shunt conductance caused by microelectrode impalement can interfere with such measurements, the passive membrane properties of the three major classes of hippocampal neurons were recently re-evaluated using patch-clamp recordings in the *in vitro* slice preparation[4]. By taking advantage of the perforated patch-clamp method, it was also possible to minimize the effects of cytoplasmic dialysis in these experiments. Using this method, both R_N and τ_0 were determined to be much larger than previous values estimated from conventional microelectrode recordings (see Table I), indicating that R_m is substantially higher than previously thought.

The ratio of the microelectrode:patch-clamp values of R_N and τ_0 shown in Table I indicate that values of R_N derived from microelectrode recordings are smaller with respect to the patch-clamp values than are the τ_0 values. This result is consistent with existing analytical models of the effect of a somatic leak on these two parameters; increasing the leak conductance at the soma produces a larger decrease in R_N than in τ_0 (Ref. 4). This finding demonstrates that the differences between patch-clamp and microelectrode estimates of R_N and τ_0 can be accounted for entirely by the dramatic reduction of a somatic leak in the patch-clamp recordings; with patch-clamp elec-

TABLE I. Input resistance and membrane time-constant values

	CA1	CA3	DG
R_N (MΩ)			
microelectrode	35.4	36.0	45.2
perforated patch-clamp	104	135	446
ratio (micro/patch)	0.34	0.27	0.10
τ_m (ms)			
microelectrode	14.6	21.9	10.8
perforated patch-clamp	28	66	43
ratio (micro/patch)	0.52	0.33	0.25

Input resistance (R_N) and membrane time constant (τ_m) values determined at the resting potential using microelectrode and perforated patch-clamp recordings from neurons in area CA1, area CA3 and the dentate gyrus (DG) of the hippocampus. Microelectrode values are mean values reported in Refs 5–8. Table adapted from Ref. 4.

Box 1. Methods for analysing electrotonic structure

A. Equivalent cylinder representation of dendrites

The first method developed for treating the electrotonic structure of branching dendritic trees in a manageable way was the equivalent cylinder model developed by Rall[a]. Using this method, the dendritic tree can be collapsed to a single cylinder, characterized by its electrotonic length (L), which is defined as:

$$L = l/\lambda \quad (1)$$

where l is the length of the equivalent cylinder (usually given in cm) and λ is the space constant (also in cm), which is calculated as:

$$\lambda = \sqrt{\frac{aR_m}{2R_i}} \quad (2)$$

where a (in cm) is the radius of the cable and R_m is the specific membrane resistivity (in Ωcm^2), and R_i the internal resistivity (in Ωcm). In physical terms, λ is the distance along an infinite cylinder (with the same a, R_m and R_i) over which a steady-state voltage decays e-fold; L is the number (or fraction) of λ in the length of the equivalent cylinder, but since the cable is finite, voltage decays less than e-fold per λ. The charging of the membrane of such a neuron can be described as an infinite sum of exponentials:

$$V = A_0 e^{-t/\tau_0} + A_1 e^{-t/\tau_1} + \ldots \quad (3)$$

where A_0, A_1, τ_1, τ_2, etc. are the amplitudes and time constants, respectively, of the terms in the series. The slowest time constant, τ_0, is equal to the membrane time constant τ_m, which can be further defined as:

$$\tau_m = R_m C_m \quad (4)$$

where C_m is the specific membrane capacitance (in $\mu F/cm^2$). Equations have also been described for determining L from the first two membrane charging time constants (τ_0 and τ_1 in Eqn 3)[a,b].

Early estimates of L for many types of neurons are likely to be wrong because of the large contribution of the microelectrode impalement-induced leak conductance to the membrane charging time constants used to derive these estimates[c,d]. Even with patch-clamp recordings, estimates of L can be in error owing to the difficulty in extracting the appropriate time constants from the infinite series of exponentials that theoretically determine membrane-charging and because of the lack of uniform L for all dendritic branches[c–e].

B. Compartmental models

The second class of models described by Rall for the analysis of electrotonic structure is compartmental models (reviewed in Ref. f). In such models, the dendritic tree is divided into segments, or compartments, each of which is treated as a linear cable. Solutions for the changes in voltage in response to current injection can be solved analytically for the passive case (most recently, Ref. c). Using a system of differential equations, numerical solutions can also be determined for either current injection or conductance changes in both the passive and active cases. A number of general-purpose computer programs has made this method particularly popular[g].

C. Multiple equivalent cylinders

Recently, methods have also been described for representing neurons as multiple equivalent cylinders[h]. This type of model extends the concept of the equivalent cylinder model to neurons whose dendrites do not all end at the same electrotonic length. In addition, such models allow for many of the functional properties of the dendrites to be preserved while greatly simplifying the dendritic tree and reducing the time required for computation of voltages in the dendrites in response to an input[i,j].

D. Dendrograms, morphotonic and morphoelectrotonic transforms

Each of these methods facilitates comparison of the anatomical and electrical structure of branches within a dendritic tree as well as comparison of the structure of dendritic trees from different neurons. In the dendrogram, each branch of a dendrite is represented by a line corresponding to its diameter and physical length from the soma[k,l]. Similarly, the morphotonic transform displays dendrites using lines corresponding to electrical distance from the soma[l]. In the morphoelectrotonic transform, the electrical properties of a neuron are displayed as a conventional morphological drawing where anatomical length has been transformed to correspond to one of a number of possible electrical transfer functions such as steady-state decay of potential from the soma to the dendrite or decay of an EPSP from the dendrite to the soma[m].

References

a Rall, W. (1977) in *Handbook of Physiology. The Nervous System. Cellular Biology of Neurons*, Section 1, Vol. I, pp. 39–97, American Physiological Society
b Johnston, D. (1981) *Cell. Mol. Neurobiol.* 1, 41–55
c Major, G., Evans, J. D. and Jack, J. J. B. (1993) *Biophys. J.* 65, 423–449
d Holmes, W. R. and Rall, W. (1992) *J. Neurophysiol.* 68, 1421–1437
e Holmes, W. R., Segev, I. and Rall, W. (1992) *J. Neurophysiol.* 68, 1401–1420
f Segev, I., Fleshman, J. W. and Burke, R. E. (1989) in *Methods in Neuronal Modeling: From Synapses to Networks* (Koch, C. and Segev, I., eds), pp. 63–96, MIT Press
g De Schutter, E. (1992) *Trends Neurosci.* 15, 462–464
h Stratford, K., Mason, A., Larkman, A., Major, G. and Jack, J. (1989) in *The Computing Neuron* (Durbin, R., Miall, C. and Mitchinson, G., eds), pp. 296–321, Adison-Wesley
i Bush, P. C. and Sejnowski, T. J. (1993) *J. Neurosci. Methods* 46, 159–166
j Segev, I. (1992) *Trends Neurosci.* 15, 414–421
k Fleshman, J. W., Segev, I. and Burke, R. E. (1988) *J. Neurophysiol.* 60, 60–85
l Larkman, A. U., Major, G., Stratford, K. J. and Jack, J. J. B. (1992) *J. Comp. Neurol.* 323, 137–152
m Tsai, K., Carnevale, N. T., Claiborne, B. J. and Brown, T. H. *Network* (in press)

trodes, seal resistances are normally 10–100 times higher than R_N, both in the cell-attached mode and following break-in and subsequent formation of an outside-out patch. The difference in the effects of a leak on R_N and τ_0 is a consequence of the non-isopotential structure of hippocampal neurons, since the effects of a leak on these two parameters are equal in isopotential models[4,9].

Internal resistivity and electrotonic structure

In addition to R_m and morphology, neuronal electrotonic structure is determined also by the internal

resistivity, R_i. Although this parameter is difficult to measure directly, a number of modeling studies are beginning to converge on the consensus that R_i is likely to be much larger than the value of 50–100 Ωcm accepted earlier. Recent estimates of 200–400 Ωcm

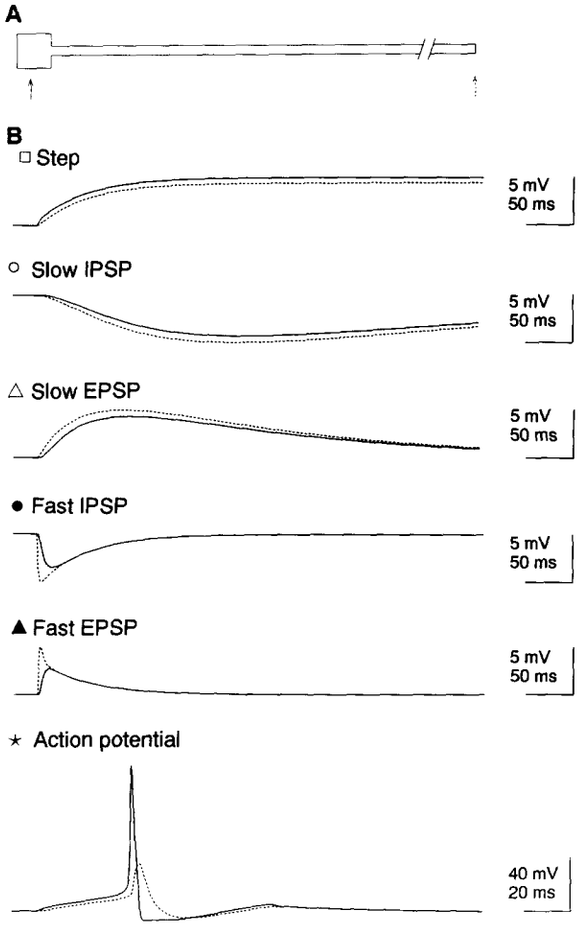

Fig. 1. *Attenuation of membrane potential changes in a cable model is larger for transient events than for steady-state events.* **(A)** *Schematic diagram of the equivalent cylinder model used. The model is drawn to scale, except for the length of the cable, which is actually five times longer than shown here (as indicated by break). The following parameters were modeled to create a cable with* $L = 0.5$*: cable diameter = 1.6 μm; cable length = 500 μm;* $R_m = 50000\ \Omega cm^2$ *and* $R_i = 200\ \Omega cm$*. The soma connected to one end of the cable was modeled using a standard cylindrical compartment with a length and diameter of 10 μm. Arrows indicate the positions of the voltage traces shown below.* **(B)** *Simulated membrane potential changes at the soma (solid traces) and at the end of the cable (broken-line traces). Note that all traces are on the same timescale, except for the action potential. The step and action potential responses were simulated by injecting rectangular current pulses at the soma (which therefore decay as they propagate to the end of the cable). The action potential was generated using* Na^+ *and* K^+ *conductances located exclusively at the soma. All synaptic events were simulated at the end of the cable (and therefore decay as they propagate to the soma) using a conductance change modeled by the sum of a single-exponential rise and a single-exponential decay with values chosen to approximate the kinetics of synaptic events. Simulations were performed using NEURON (Ref. 12).*

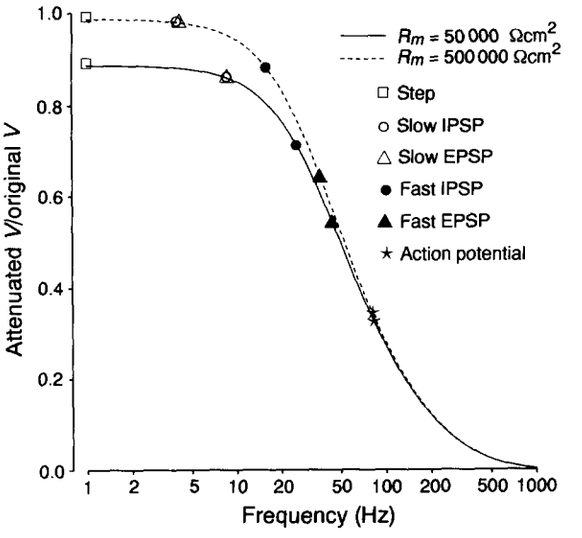

Fig. 2. *Voltage attenuation in a cable is frequency-dependent. Attenuation of sine-wave voltage changes of 1–1000 Hz were calculated for the model shown in Fig. 1A using published equations[14,15]. The attenuation ratio is plotted as a function of frequency. The plot shows that high-frequency voltage changes are attenuated much more than low-frequency voltage changes. The attenuation of physiological events is shown by plotting these events at frequencies where they fall on the lines for sine-wave attenuation. Note that the attenuation of a step is slightly less than that of the lowest frequency sine wave shown here (1 Hz). Increasing* R_m *from 50000 Ωcm²* *(solid line) to 500000 Ωcm²* *(broken line) reduces the attenuation of low-frequency voltage changes much more than that of high-frequency voltage changes. In addition, the slowing of the decay of EPSPs and IPSPs by the increase in* R_m *decreases the attenuation of these events.*

are suggested by various attempts to fit physiological data with models incorporating anatomical data[3,4,10,11]. These higher values of R_i imply that central neurons are likely to have substantial values of L, despite the higher estimates of R_m.

Attenuation of synaptic potentials in dendrites

A simple equivalent cylinder model is used in Fig. 1 to illustrate how voltage transients with different timecourses are attenuated and filtered by the dendrite. The model is generic in the sense that it is not meant to represent any particular type of neuron, although the parameter values chosen (see legend) are loosely based on data from hippocampal neurons[4].

The propagation of potentials in dendrites is known to be very frequency-dependent, with faster events being attenuated to a much greater extent than slower or steady-state voltage changes[13–15]. The importance of this fact has been overlooked by many investigators; neurons having values of L less than one are often referred to as 'electrotonically compact'. As shown in Fig. 1B, for a neuron with a value for L of 0.5 the steady-state voltage response to a step of current is only nominally attenuated, but faster events such as action potentials and fast synaptic potentials are substantially attenuated. Slow EPSPs and slow IPSPs undergo an intermediate amount of attenuation. The relationship between the attenuation of a voltage change and its frequency is shown in Fig. 2. The symbols on this plot indicate the amount of

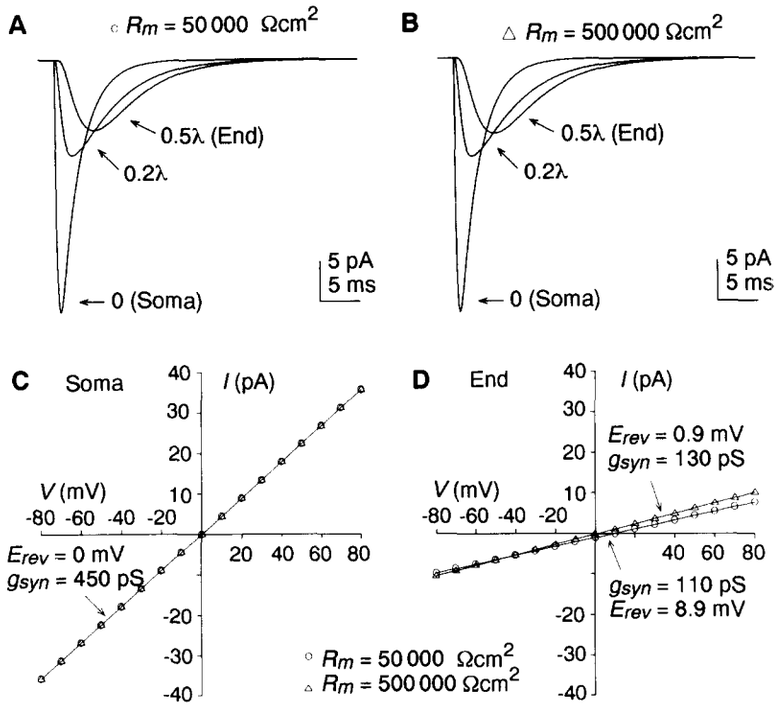

Fig. 3. *Increasing R_m improves reversal potential measurement while producing only a nominal improvement in peak current and slope conductance measurements.* **(A)** *Currents measured with a somatic voltage clamp when synapses were activated at different locations on the model shown in Fig. 1A (R_m = 50 000 Ωcm²). The synaptic conductance change is identical to that underlying the fast EPSP shown and described in Fig. 1.* **(B)** *Currents measured with a somatic voltage clamp in the same model, but with an increased membrane resistivity (R_m = 500 000 Ωcm²). The attenuation of peak current for remote synapses is hardly affected by the increase in R_m.* **(C)** *The current–voltage plot for the synapse at the soma results in the correct measured slope conductance of 450 pS and reversal potential of 0 mV for both R_m values.* **(D)** *The current–voltage plot for the synapse at the end of the cable yields much lower measured slope conductances. While the measured reversal potential with the high R_m value is close to the real value, the increased R_m produces only a slight improvement in the measured slope conductance, which is still only about one-quarter of the real value.* Figure adapted from Ref. 15.

attenuation of the peak amplitude of the physiological events from Fig. 1B. The action potential is attenuated by 67%, about the same as the attenuation of a sine wave of 83 Hz, while the slow IPSP is attenuated only 14%, about the same as a 9 Hz sine wave.

The amount of attenuation of a given voltage change is also dependent on R_m, which is determined by the type and density of ion channels in the membrane that are open near the resting potential. Experimentally, R_m can be increased by blocking K^+ channels (for example, by filling neurons with Cs^+). Figure 2 shows that the reduction in attenuation caused by such increases in R_m is greater at lower frequencies. The effect of a change in R_m on the attenuation of any event results from two factors: the change in electrotonic distance and the effect of R_m on the timecourse of the event (see Eqns 3 and 4, Box 1). The reduction in attenuation of PSPs by an increase in R_m is therefore due to both a reduction of the electrotonic length of the neuron and a slowing of the timecourse of the event. In contrast, the timecourse of an action potential is only slightly affected by changes in R_m. This, combined with the fact that the action potential is very fast, accounts for an increase in R_m having very little effect on action potential attenuation (see Fig. 2).

Attenuation of measured synaptic currents: space-clamp problems

The frequency-dependent attenuation of voltage in dendrites has important implications for measuring synaptic currents using a voltage-clamp at the soma. If the membrane potential at the synapse is indeed clamped, then both the amplitude and timecourse of the current measured by the clamp reflect the real postsynaptic current (PSC), which is independent of R_m and is determined by other factors such as the kinetics of the transmitter-gated ion channels and the timecourse of transmitter in the synaptic cleft (see Ref. 16 for review). Most synapses in the CNS, though, are located in the dendrites at distances where it is impossible to achieve perfect voltage control with a somatic voltage-clamp. Under these conditions, this so-called 'space-clamp' problem is affected by R_m in two ways, which are considered in turn below.

First, consider the effect on R_m of the ability to voltage clamp a synaptic event in the dendrites. Higher R_m values (as observed with patch-clamp recording and the use of intracellular Cs^{2+} imply a shorter steady-state electrotonic distance of the synapse. This improves the situation for voltage clamping very slow synaptic currents, but not for faster events. This is demonstrated in Fig. 3A, which shows simulated currents measured in response to activation of identical fast excitatory synapses located at different distances from a somatic voltage clamp. As shown here, even synapses located relatively close to the soma are susceptible to severe attenuation and filtering as a result of inadequate space clamp.

Increasing R_m provides practically no improvement in the space clamp of these same synaptic events (Fig. 3B). The current–voltage relations for the somatic synapse (Fig. 3C) and the identical synapse placed at the end of the cable (Fig. 3D) show that, while increasing R_m by a factor of ten improves the measured reversal potential (E'_{rev}) of the poorly clamped event, only a small improvement in the measured synaptic conductance is achieved. This occurs because E'_{rev} is determined exclusively by the steady-state, soma-to-synapse electrotonic distance (which is substantially reduced by a tenfold increase in R_m), while the peak current is determined by the transient attenuation properties (which are relatively insensitive to changes in R_m). This is an important point because it demonstrates that a measured reversal potential close to the expected value is not a good test of the adequacy of the voltage clamp. Similarly, methods that attempt to compare the rate of a 'clamped' synaptic event to the rate of clamp settling[17] or to the time constant for turn-off of an NMDA EPSC (in response to a voltage step at the soma)[18] are unreliable. It is possible for a fast PSC to be filtered such that it becomes slower than either of these two measures. However, the latter method could prove to be an excellent way to estimate the electrotonic location of activated synapses.

The second effect of R_m on poorly-clamped PSCs is on the timecourse of the measured event. Increasing R_m increases τ_m and therefore slows the decay of the membrane potential at the synapse that escapes the somatic voltage clamp and is therefore referred to as the 'escape voltage'. Since the voltage clamp

continues to pass current as long as a change in membrane potential is detected, increasing R_m can actually have the undesirable effect of slowing the measured synaptic current[15].

The effects of space-clamp errors in a more morphologically realistic model than the equivalent cylinder model are shown in Fig. 4. Here, identical fast excitatory synapses at a range of electrotonic locations corresponding to mossy fiber (MF), commissural–associational (C–A) and perforant-path (PP) synapses are simulated in a compartmental model of a hippocampal CA3 pyramidal neuron. The currents measured with a somatic voltage clamp are shown in the left panel. Clearly, the C–A and PP synaptic currents are severely distorted when compared to the somatic synapse, which is perfectly clamped. Synaptic currents from the MF synapses (which occur quite close to the soma) are much less distorted. The inability of a somatic electrode to voltage-clamp synapses not located at the soma is shown by the escape voltage that occurs at the synapse. For comparison, the amplitudes of the EPSPs (measured under current-clamp conditions) at each of the synaptic sites are illustrated by the broken lines on the right. It is interesting to note that the change in potential found in the dendrites during distal synaptic events is virtually unaffected by the presence of a voltage clamp at the soma and that the timecourse of the measured synaptic current more accurately reflects that of the EPSP than that of the true EPSC.

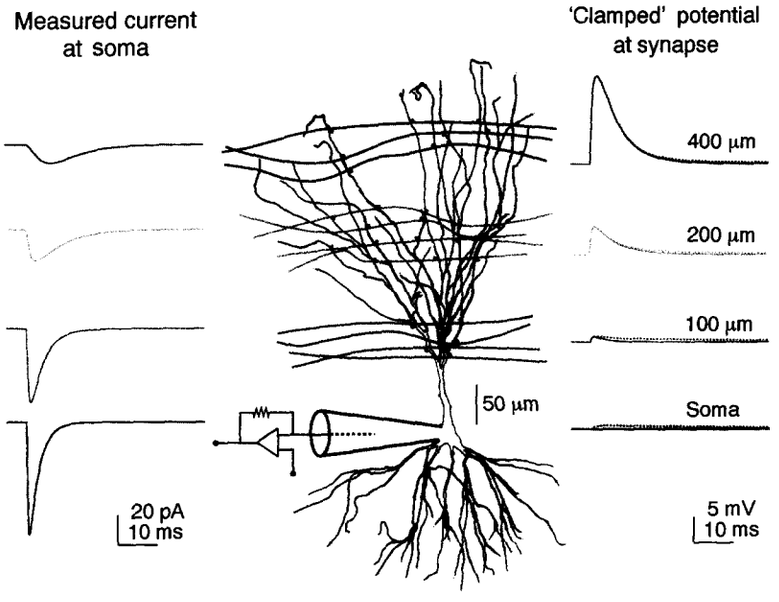

Fig. 4. *Voltage- and space-clamp error in currents measured with a somatic voltage-clamp in a realistic compartmental model of a CA3 pyramidal neuron. Fast excitatory synapses modeled using an identical conductance change to that described in Fig. 1 were simulated at four different locations in the model. The measured currents (left) are clearly filtered and attenuated in comparison to the perfectly-clamped synapse (at the soma). The inability of the somatic electrode to clamp the membrane potential at the synapse is shown by the records of synaptic escape voltage (solid lines in right column; mean distances of the synapses from the soma are indicated). The unclamped EPSPs (broken lines in right column) are also shown for comparison. Note that the EPSPs in the distal dendrites are essentially unaffected by the somatic clamp.* Figure adapted from Ref. 15.

Other membrane properties shaping synaptic responses

The examples illustrated in Figs 1–4 use completely passive models, but a detailed understanding of the attenuation of synaptic events and other aspects of synaptic integration will require the extension of such models to include voltage-gated channels both in the dendrites and the soma. These channels are likely to shape PSPs in more complex ways, the effects of which can be examined experimentally and with compartmental models and visualized using methods such as morphoelectrotonic transforms (see Box 1).

Recent data have offered some insight into the diversity of the types and distributions of ion channels contributing to both the passive and the active properties of dendrites. Evidence from perforated patch-clamp recordings of hippocampal neurons has shown that R_N and τ_0, although defined as 'passive' properties, are in fact dependent on the membrane potential. In all three classes of hippocampal neurons both R_N and τ_0 are larger at relatively depolarized potentials and smaller at relatively hyperpolarized potentials[4]. This is likely to be the result of voltage-gated ion channels opened by hyperpolarization. The sensitivity of R_N and τ_0 to small changes in both directions around the resting potential suggests that these channels are open at the resting potential and contribute to the measured value of R_m (Ref. 4). In cortical pyramidal neurons, it has been shown that dendritic channels activated by hyperpolarization can affect the shape of the EPSP (Ref. 14).

Voltage-gated Na^+ and Ca^{2+} channels activated by depolarization have also been shown to exist in the dendrites of some neurons[20,21] and can be activated by synaptic stimulation[22,23]. To what extents these channels are activated during physiological synaptic activity and how they shape the resulting PSP are important issues that will undoubtedly be the subjects of many future studies. Equally interesting is the role that passive voltage attenuation plays in determining the pattern of activation of these channels. For example, in hippocampal pyramidal neurons it has been shown that attenuation of the action potential normally prevents the activation of Ca^{2+} channels in the distal dendrites, but that these channels are activated if the depolarization is prolonged so that it propagates more effectively to these regions of the dendrites[20].

Voltage-gated channels in dendrites might further complicate attempts to measure current from remote synapses with a somatic voltage-clamp. Because of the space-clamp problems discussed above, voltage changes at poorly clamped synapses could be large enough to activate voltage-gated channels, thus contributing a non-synaptic component to the measured current.

Finally, it is important to point out that changes in the effective R_m value could occur through activation of ligand- or voltage-gated channels or modulation of ion channels by second-messenger systems. Such changes could occur either in large parts of the dendritic tree (for example, by synaptic bombardment[24] or diffuse release of neurotransmitters or neuromodulators) or very locally (for example, by GABA-mediated 'shunting' inhibition or activation of K^+ channels following action potentials). In this way, PSP shape could be altered by changes in the electrotonic structure of the dendritic tree, changes in the

Acknowledgements *The authors thank Greg Stuart, Michael Häusser and Ted Carnevale for critical comments on the manuscript. This work was supported by grants from the National Institutes of Mental Health (MH44754 and MH48431) and the Keck Foundation. Nelson Spruston also thanks Bert Sakmann and the Alexander von Humboldt Foundation for support.*

timecourse of synaptic potentials, or by changes in the active response to synaptically-mediated membrane potentials.

Concluding remarks

Experiments using patch-clamp recordings from hippocampal neurons have revealed higher R_N and longer τ_0 values than were determined previously using microelectrode recordings. These new estimates of passive membrane properties have important implications for determining the shape and attenuation of PSPs but do not, as some have argued, mean that synapses in dendrites can be adequately voltage-clamped using somatic electrodes. Understanding the nature of the ion channels underlying both passive and active membrane properties of neurons is an important step toward understanding how information from thousands of synaptic inputs is integrated in the dendritic tree.

Selected references

1 Rall, W. (1977) in *Handbook of Physiology. The Nervous System. Cellular Biology of Neurons*, Section 1, Vol. I, pp. 39–97, American Physiological Society
2 Holmes, W. R., Segev, I. and Rall, W. (1992) *J. Neurophysiol.* 68, 1401–1420
3 Major, G., Larkman, A. U., Jonas, P., Sakmann, B. and Jack, J. J. B. *J. Neurosci.* (in press)
4 Spruston, N. and Johnston, D. (1992) *J. Neurophysiol.* 67, 508–529
5 Johnston, D. (1981) *Cell. Mol. Neurobiol.* 1, 41–55
6 Brown, T. H., Fricke, R. A. and Perkel, D. H. (1981) *J. Neurophysiol.* 46, 812–827
7 Durand, D., Carlen, P. L., Gurevich, N., Ho, A. and Kunov, H. (1983) *J. Neurophysiol.* 50, 1080–1097
8 Turner, D. A. and Schwartzkroin, P. A. (1983) *J. Neurosci.* 3, 2381–2394
9 Holmes, W. R. and Rall, W. (1992) *J. Neurophysiol.* 68, 1421–1437
10 Major, G., Evans, J. D. and Jack, J. J. B. (1993) *Biophys. J.* 65, 423–449
11 Shelton, D. P. (1985) *Neuroscience* 14, 111–131
12 Hines, M. A. (1989) *Int. J. Biomed. Comput.* 24, 55–68
13 Johnston, D. and Brown, T. H. (1983) *J. Neurophysiol.* 50, 464–486
14 Rall, W. and Segev, I. (1985) in *Voltage and Patch-clamping with Microelectrodes* (Smith, T. G., Jr, Lecar, H. and Redman, S. J., eds), pp. 191–215, American Physiological Society
15 Spruston, N., Jaffe, D. B., Williams, S. W. and Johnston, D. (1993) *J. Neurophysiol.* 70, 781–802
16 Jonas, P. and Spruston, N. *Curr. Opin. Biol.* (in press)
17 Llano, I., Marty, A., Armstrong, C. M. and Konnerth, A. (1991) *J. Physiol.* 434, 183–213
18 Hestrin, S., Nicoll, R. A., Perkel, D. J. and Sah, P. (1990) *J. Physiol.* 422, 203–225
19 Nicoll, A., Larkman, A. U. and Blakemore, C. (1993) *J. Physiol.* 468, 693–710
20 Jaffe, D. B. *et al.* (1992) *Nature* 357, 244–246
21 Stuart, G. J. and Sakmann, B. (1994) *Nature* 367, 69–72
22 Miyakawa, H. *et al.* (1992) *Neuron* 9, 1163–1173
23 Markram, H. and Sakmann, B. *Proc. Natl Acad. Sci. USA* (in press)
24 Bernander, O., Douglas, R. J., Martin, K. A. and Koch, C. (1991) *Proc. Natl Acad. Sci. USA* 88, 11569–11573

Processing of information from different sources: spatial synaptic integration in the dendrites of vertebrate CNS neurons

J. Midtgaard

J. Midtgaard is at the Division of Neurophysiology, Dept of Medical Physiology, University of Copenhagen, Blegdamsvej 3, DK 2200 N Copenhagen, Denmark.

Most synapses on a neuron are distributed along the dendrites. Inputs from different types of presynaptic neurons often distribute to different dendritic compartments. This provides an anatomical framework for spatial synaptic integration. At the same time, a plethora of time- and voltage-dependent responses are present, usually with a distinct distribution over the somato–dendritic membrane. These intrinsic conductances shape the local dendritic response to ligand-gated conductances, and provide the dendrites with a dynamic way of regulating the interaction between synapses. Recent results from neurons in the vertebrate CNS exemplify these mechanisms of dendritic integration.

Classically, spatial synaptic integration is defined as the summation of synaptic potentials, which are generated in different parts of the cell, at the output region of the cell. Usually the integration then determines the occurrence of all-or-none, propagated axonal action potentials[1]. The concept of spatial integration is expanded by the presence of dendritic voltage-dependent channels[1,2] and each location containing such channels becomes a focal point for synaptic integration. Spatial dendritic integration is determined by the location and strength of synapses in combination with the dendritic cable properties[2,3], which separate synapses biochemically and electrically[4–6]. A large variety of ion conductances gated by membrane potential or by intracellular Ca^{2+} are found in vertebrate neurons[4,7–9]. In addition to the conductances of ion channels gated by direct binding of neurotransmitters or via second messengers such as G proteins, these intrinsic conductances serve to characterize each type of neuron. The intrinsic conductances are inhomogenously distributed over the somato–dendritic membrane, giving each compartment distinct electrophysiological properties[8]. The concerted action of the ion channels determines the cell-specific firing pattern; the distribution of active properties becomes significant as synapses from different types of presynaptic neurons are distributed among different dendritic compartments. This means that both the local synaptic response as well as interactions along the dendrites can be influenced by the intrinsic properties.

Several theoretical studies have addressed spatial integration, for example, models of active membrane properties of spines and dendrites[2–4,10,11]. Recently, spatial integration in vertebrate central neurons has come under direct experimental scrutiny by the use of intradendritic microelectrode recordings and by the advent of imaging techniques with high spatial and temporal resolution. Rather than reviewing the pharmacological and molecular properties of receptors